ELSEVIER

Contents lists available at ScienceDirect

Journal of Hydrology

journal homepage: www.elsevier.com/locate/jhydrol





Real-time bioluminescent imaging of spatiotemporal variation of microbial retention during transport through porous media under variably saturated flow conditions

Liqiong Yang ^{a,b}, Jia Kang ^a, Xijuan Chen ^a, Steven A. Ripp ^c, William P. Johnson ^{d,*}, Jie Zhuang ^{c,e,*}

- a Key Laboratory of Pollution Ecology and Environmental Engineering, Institute of Applied Ecology, Chinese Academy of Sciences, Shenyang, Liaoning Province 110161,
- ^b College of Resources and Environment, University of Chinese Academy of Sciences, Beijing 100864, China
- ^c Center for Environmental Biotechnology, The University of Tennessee, Knoxville, TN 37996, USA
- ^d Department of Geology & Geophysics, The University of Utah, Salt Lake City, UT 84112, USA
- ^e Department of Biosystems Engineering and Soil Science, The University of Tennessee, Knoxville, TN 37996, USA

ARTICLE INFO

This manuscript was handled by J. Simunek, Editor-in-Chief, with the assistance of Kathleen M Smits. Associate Editor

Keywords:
Bacterial transport
Unsaturated flow
Real-time bioluminescent imaging
Flow velocity

ABSTRACT

This study investigated the transport and retention of bioluminescent Escherichia coli strain 652T7 under different pore water velocities (8.7 cm h^{-1} and 13.0 cm h^{-1}) and pore water saturations (85% and 100%) utilizing a noninvasive, real-time bioluminescent imaging technique. Under saturated flow conditions, the concentrations of retained bioluminescent E. coli 652T7 decreased exponentially with distance from the source at the lower velocity but decreased non-exponentially at the higher velocity. Under unsaturated flow conditions, pore water velocity had no significant effect on bacterial breakthrough concentration; however, the concentrations of retained cells were maximal at a significant distance from the source (non-monotonic). The distance from source of the maximum concentration increased from 2.4-cm at 1.05 pore volumes to 4.3-cm at 3.15 pore volumes, indicating slow translation of bacterial down-gradient under unsaturated flow conditions. That conditions were modestly unfavorable to attachment at the solid-water interface (SWI) was indicated by deposition rate coefficients being greater (by a factor of four) for simulations versus experiments, and by significant repulsive barriers to attachment at both the SWI (260 kT) and the air-water interface (AWI, fully repulsive). The inferred slow translation under unsaturated flow conditions therefore reflects either accumulation without arrest in the secondary minimum at the SWI and/or capillary interaction at the AWI. This non-invasive bioluminescence method yielded real-time quantitative observation of bacterial distribution from source and demonstrated contrasting transport behaviors previously obtained solely via more laborious methods with limited spatio-temporal observation.

1. Introduction

An improved understanding of processes that control the transport, retention, and release of bacteria in porous media is needed for a variety of environmental and industrial applications such as bioremediation of contaminated soils and aquifers and filtration of pathogenic microorganisms in groundwater or engineered water treatment systems (Redman et al., 2004; Liu et al., 2007; Bai et al., 2016; Sasidharan et al., 2017; Adadevoh et al., 2018). In addition, the knowledge of in-situ spatial distribution of bacteria during their transport through heterogeneous

porous media is required for accurate prediction of bacterial break-through behaviors (Tong et al., 2005; Keller and Auset, 2007; Rockhold et al., 2007; Bradford and Torkzaban, 2008; Engström et al., 2015). However, the mechanisms of bacterial transport and retention in porous media are complex and predictive capability is limited (e.g., Molnar et al., 2015). For instance, traditional colloid filtration theory assumes an exponential decrease in retained bacterial concentrations with transport distance (e.g., Yao et al., 1971; Logan et al., 1995; Tufenkji and Elimelech, 2004). However, under some conditions retained bacteria frequently exhibit a distance-dependent deposition rate coefficient that

^{*} Corresponding authors at: Department of Biosystems Engineering and Soil Science, The University of Tennessee, Knoxville, TN 37996, USA (J. Zhuang). E-mail address: jzhuang@utk.edu (J. Zhuang).

decreases with transport distance) (multi-exponential) (Bolster et al., 2000; Redman et al., 2001; Firouzi et al., 2015; Zhang et al., 2016; Balkhair, 2017; Ma et al., 2018) or one that increases then decreases to produce a maximum concentration down-gradient from the injection source) (Tong et al., 2005; Bradford et al., 2006; Johnson et al., 2018). The above-cited research primarily pertains to saturated porous media, and less is known about the spatial distribution of bacteria during their transport and retention in unsaturated porous systems.

The above-described behaviours (Aramrak et al., 2011, 2014, Gómez-Suárez et al., 1999, 2000; Lazouskaya et al., 2011; Noordmans et al., 1997; Sharma et al., 2008) were investigated in packed columns by dissecting the column following the end of the experiment. In these experiments, the role of attachment versus retention without attachment in secondary minima was elucidated using replicate columns dissected following contrasting numbers of pore volumes (e.g., Tong et al., 2005) and through direct pore-scale observation in micromodels (e.g., Tong and Johnson, 2006; Keller and Auset, 2007). Thus far, no method produces real-time in-situ information regarding bacterial retention at column scale (Zhuang et al., 2020). The primary objective of this study was to examine real-time in-situ transport and retention of a constitutively bioluminescent *Escherichia coli* strain in porous media using a novel real-time bioluminescent imaging system.

2. Materials and methods

2.1. Bacteria and culture conditions

This study was performed using the constitutively bioluminescent Escherichia coli strain 652T7, which consists of a T7 promoter fusion to the Photorhabdus luminescens luxCDABE gene cassette (Shi et al., 2014). E. coli 652T7 subsequently generates a continuous 490 nm light signal. A PerkinElmer IVIS Spectrum was used to measure and capture bioluminescence emission in real-time from strain 652T7 during its transport and retention in a sand column. The strain was cultured in a sterile 250 mL baffled shake flask containing 100 mL of Luria Bertani (LB) with a final kanamycin (CAS 133–92-6) concentration of 10 mg L^{-1} . The cells were cultured in a rotary shaker (HZQ-X160) at 160 rpm and 37 °C. The culture was grown to stationary phase (optical density of 1.0 at a wavelength of 600 nm), centrifuged at 1000 g for 10 min, and resuspended in 100 mM NaCl, pH 6.5 (background solution). The cell length and zeta potentials of E. coli 652T7 were measured in triplicate using a laser particle analyzer (Brookhaven, 90Plus Zeta) in the same background solution as used for the column experiments (n > 50). Cellsurface hydrophobicity was derived from the contact angles using a goniometer microscope (Krüss GmbH, Germany). No significant differences were observed for the cell length (1.7 \pm 0.4 μ m), cell zeta potential (-25.6 \pm 2.1 mV) and contact angle (25 \pm 3°) in different column experiments (Student's t-test, p > 0.05).

2.2. Column experiments

The column assembly was comprised of a glass chromatography column (diameter of 3.8 cm, length of 10 cm) containing a 40–60 mesh quartz sand (Kermel, China, AR) at a porosity of \sim 0.37. Prior to the experiments, the sand was washed in HCl (10 mM) and then NaOH (10 mM) solutions to remove suspended impurities and then finally rinsed with deionized water. The column was closed at one end with an 80 mesh nylon membrane and then dry-packed with the cleaned sand in 1 cm increments with stirring and tapping. After packing, the other end similarly received an 80 mesh nylon membrane closure. High pressure $\rm CO_2$ gas was then introduced into the column at a low flow rate for 6 h to displace trapped air. The packed column was thereafter flushed upward with 20 pore volumes of sterilized NaCl background solution at the same pore water velocity as the bacterial transport, either 8.7 cm h $^{-1}$ or 13.0 cm h $^{-1}$. Under the saturated flow conditions, only one peristaltic pump was used to inject bacteria. Under unsaturated flow conditions, a piston

pump and a sprinkler head were connected to the top of the column to facilitate inflow of the bacterial culture, while another peristaltic pump was connected to the bottom of the column to steadily extract the liquid arriving at the outlet. Specifically, the column was first saturated by introducing the background solution. Then, the lower peristaltic pump and upper piston pump were used in cooperation to desaturate the packed porous media to a saturation level of 85%. An electronic scale was placed under the column system to monitor the change in water content. The liquid amount of one pore volume under the saturated flow conditions was estimated by subtracting the solid volume of sand packed in the column from the total inside volume of the column. The liquid volume of one pore volume under the unsaturated flow conditions was calculated by multiplying the saturated pore volume by pore water saturation. The flow of the pump was decreased under unsaturated conditions to match the same pore water velocity under saturated situations. All the column experiments excluded elution process.

Once a column was packed, it was placed vertically in the IVIS Spectrum imaging chamber. Temperature in the chamber was set at 25 °C. A mirror was placed at an appropriate angle to enable a cooled charge-coupled device (CCD) camera to capture bioluminescence emission of the bacteria from the side of the column. Average radiance in photons sec⁻¹ cm⁻² sr⁻¹ was determined every 0.35 pore volumes (i.e., 24 min for 8.7 cm h^{-1} and 16 min for 13.0 cm h^{-1}) during the transport experiments without interruption of the bacterial injection. The resulting gray scale photographic and pseudocolor bioluminescence images were automatically superimposed, so that identification of any optical signal locating bacteria in the column was facilitated. Each experiment used a freshly packed column and all experimental runs were performed in duplicate using a setup input mode. The input concentration of E. coli 652T7 was $\sim 10^8$ cells mL $^{-1}$ in NaCl background solution. Sodium bromide (NaBr) was added to the bacterial suspension at a concentration of 30 mg L⁻¹ to serve as a conservative tracer for quantifying dispersivity and hydrodynamic conditions. Effluent samples were collected from each column at every 0.35 pore volume using a fraction collector. Each effluent sample was divided into two portions. One portion was used to analyze Br - concentration using ion chromatography (Dionex, ICS-5000) while the other portion was used to measure cell concentration simultaneously by plate counting (LB agar plates containing kanamycin at 10 mg L⁻¹) and bioluminescence determination in a 96-well microtiter plate in order to obtain breakthrough curves of bacteria. At the termination of each transport experiment, the entire 10 cm length of the column was divided into 1-cm sections and the sand from each of these sections was used to determine retained bacterial concentrations along the column profile via plate counting and their bioluminescent emission profiles as measured in the IVIS Spectrum. The ten sand segments were individually placed into 100 mL of sterile NaCl (2 mM, pH 6.5) to shake for 20 min at 160 rpm. The suspension was then transferred to a 96-well plate for bioluminescent measurements. Hourly absorbance measurements of the input bacterial concentrations and their bioluminescence intensities during the entire experimental period (\sim 3.5 h) indicated that the bacterial suspension remained stable at 2 (\pm 0.09) \times 10⁸ cells mL⁻¹. The breakthrough curves of bacteria were plotted as the relative effluent concentration (C/C₀) as a function of pore volumes of injected suspension or solution. The corresponding observed retention profiles for the bacteria were plotted as the normalized solid phase concentration (S/C_0) as a function of distance from the column inlet.

2.3. Data modeling

The transport behavior of *E. coli* 652T7 bacterial populations was modeled using HYDRUS-1D with a one-dimensional advection–dispersion equation (ADE):

$$\frac{\partial C}{\partial t} = D \frac{\partial^2 C}{\partial x^2} - v \frac{\partial C}{\partial x} - k_f c \tag{1}$$

where C is the bacterial concentration in the liquid phase (cells

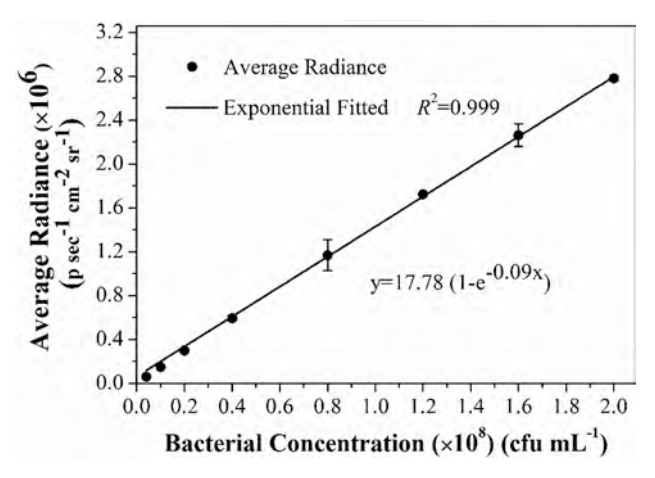


Fig. 1. Calibration curve of bioluminescence intensity against bacterial concentration determined by plate counting for *E. coli* 652T7. Error bars represent the standard deviation of two replicates. p $\sec^{-1} \operatorname{cm}^{-2} \operatorname{sr}^{-1}$ is the abbreviation of photon $\sec^{-1} \operatorname{cm}^{-2} \operatorname{steradian}^{-1}$.

mL⁻¹), t is time (h), ρ_b is the bulk density of the porous media (g cm⁻³), θ is the volumetric water content (cm³ cm⁻³), S is the bacterial concentration on porous media (cfu g⁻¹), D is the dispersion coefficient (cm² h⁻¹), x (cm) is the distance from the inlet, v is the average pore water velocity (cm h⁻¹), and k_f is the deposition rate coefficient (h⁻¹).

Under saturated steady-state conditions, we use the following equation to calculate aqueous C/C_0 as a function of distance:

$$\frac{c}{c_0} = exp\left[\left(-\frac{k_f}{v}\right)x\right] \tag{2}$$

The corresponding equation for retention in the saturated column is (Li et al., 2006):

$$S(x) = \lambda \frac{t_0 \theta k_f C_0}{\rho_h} \exp\left[-\frac{k_f}{\nu} x\right]$$
 (3)

where λ is total percentage of bacterial recovery, and t_0 is the injection duration (h).

2.4. Filtration theory

The deposition rate coefficients (k_f) was determined using the Traj-Hap model in Parti- Suite software (wpjohnsongroup.utah.edu) on the basis of filtration theory, assuming a collision efficiency (α) equal to unity (favorable conditions) to determine the value of η (collector efficiency) in the following equation:

$$k_f = \frac{3}{2} \frac{(1-\theta)}{d_c} \alpha \eta v \tag{4}$$

The value of the collector efficiency (η) can be also be determined using correlation equations approximating trajectory simulations under given conditions (e.g., Rajagopalan and Tien, 1976; Tufenkji and

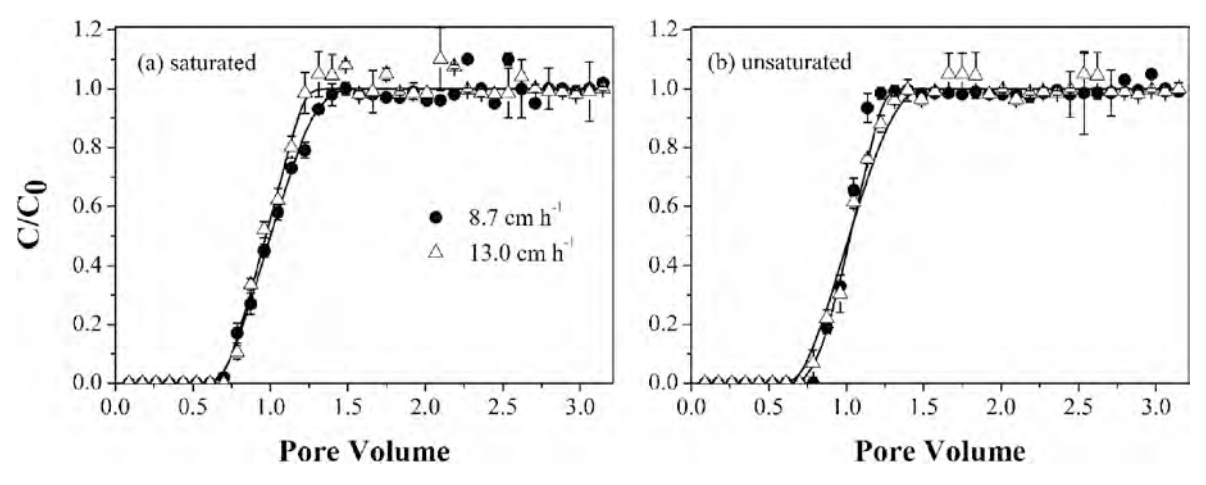


Fig. 2. Bromide breakthrough curves at different pore water velocities (8.7 cm h^{-1} and 13.0 cm h^{-1}) and under flow conditions of (a) 100% and (b) 85% water saturation. The breakthrough fitted by Hydrus-1D is shown by solid lines. Error bars represent the standard deviation of two replicates.

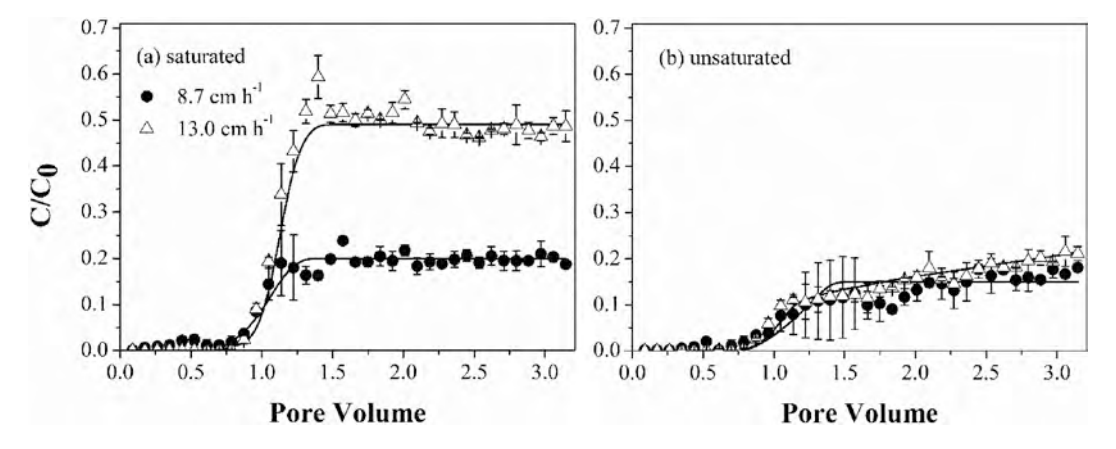


Fig. 3. Different effects of pore water velocity on the transport of *E. coli* 652T7 under flow conditions of (a) 100% and (b) 85% water saturation. The breakthrough fitted by Hydrus-1D is shown by solid lines. Error bars represent the standard deviation of two replicates.

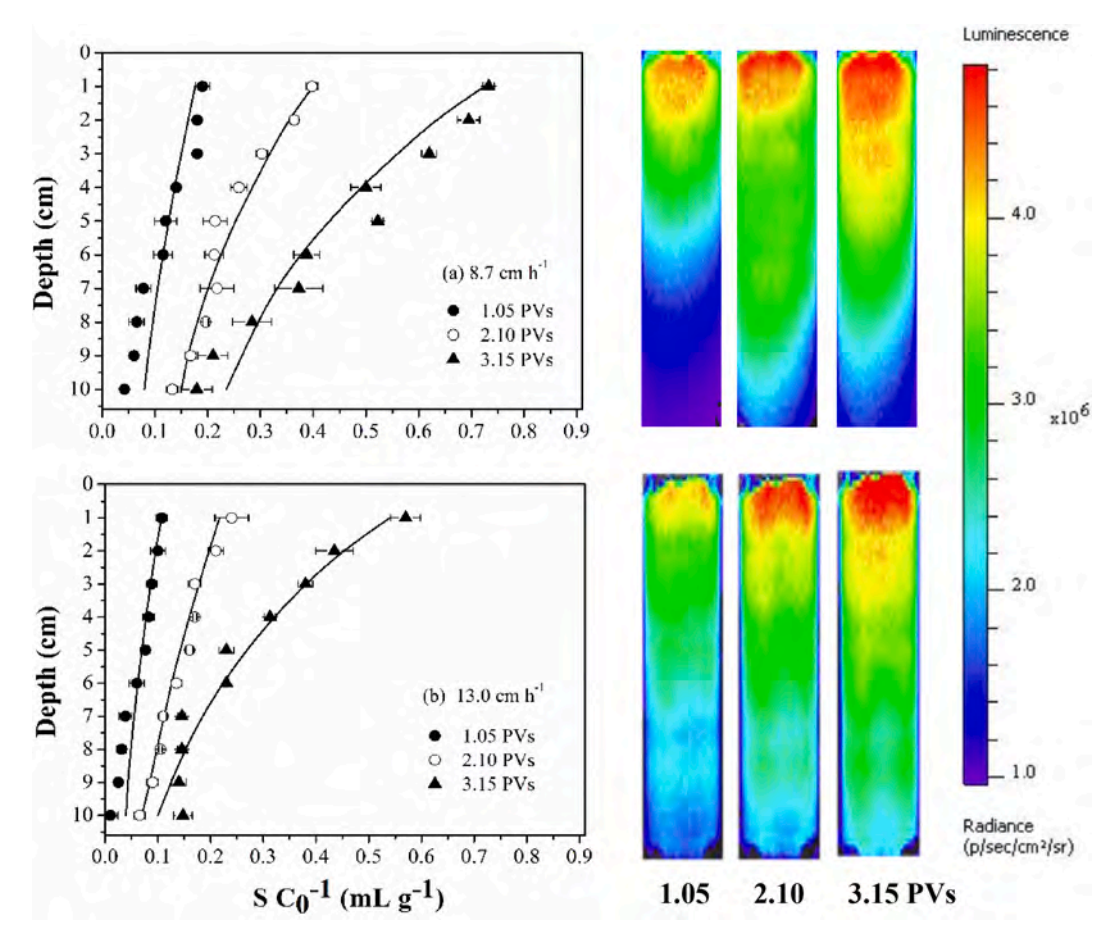


Fig. 4. The distribution of *E. coli* 652T7 with travel distance (i.e., depth) under saturated flow condition at different pore water velocities (8.7 cm h⁻¹ and 13.0 cm h⁻¹) in the porous media after 1.05, 2.10, and 3.15 pore volumes (PVs) of bacterial input. The fitted retention trend is shown by solid lines. The data (S C_0^{-1}) were acquired from the real-time images. The closer to the red part in the bioluminescent images, the higher the bacterial concentration was. Error bars represent the standard deviation of two replicates. (For interpretation of the references to colour in this figure legend, the reader is referred to the web version of this article.)

Elimelech, 2004; Long and Hilpert, 2009; Nelson and Ginn, 2011; Ma et al., 2009), and these are also available in Parti-Suite. Trajectory simulations were performed in a Happel shere-in-cell collector comprised of a spherical grain surrounded by a fluid envelope with radially symmetric divergent and convergent flow at its upstream and downstream sides, respectively, and where the thickness of the fluid envelope is equal to the difference between the collector radius (R_{HAP}) and the grain radius (R_{grain}), which are linked via the volumetric water content.

$$R_{HAP} = R_{grain} (\frac{1}{1 - \theta})^{-\frac{1}{3}}$$
 (5)

To perform trajectory simulations under unsaturated conditions, the volumetric water content defining the Happel fluid envelope thickness was set to the product of porosity and the percent saturation. The air—water interface was therefore taken as the non-tangential stress boundary on the outer boundary of the Happel fluid envelope, and although no colloid-collector interactions were simulated at this interface during the trajectory simulations, adding these interactions to that boundary is a potential future enhancement to Parti-Suite. Because colloid-interface interactions were repulsive at the air—water interface, this interaction was assumed to have negligible impact on colloid trajectories relative to bacterial-surface interactions at the sediment—water interface and capillary interactions at the air—water interface.

2.5. xDLVO interaction energy calculation

The extended Φ_{DLVO} (xDLVO) interaction energies were calculated to

elucidate the mechanisms of bacterial transport as the sum of classical DLVO and Lewis acid-base interaction energies between bacteria and sediment—water interface (SWI)/ air—water interface (AWI) by using the xDLVO module in Parti-Suite.

3. Results

3.1. Correlation of bioluminescence with optical density of E. coli 652T7

The calibration curves of bioluminescence intensity (average radiance) and bacterial concentration were established by viable plate counting (Fig. 1). The large coefficient of determination ($R^2=0.999$) indicated that the IVIS Spectrum system was acceptable for detecting bacterial concentrations.

3.2. Tracer transport

The good reproducibility of complete breakthrough of conservative bromide from all columns indicated the stability of the column system and flow conditions during the saturated and unsaturated experiments (Fig. 2). The slight difference in dispersion coefficient (*D*) estimated using the ADE equation under the same pore water saturation is attributed to the difference in pore water velocity (Table S1). The small increase in *D* value when pore water was desaturated is due to relatively larger hydrodynamic dispersion in unsaturated, less connected pores, yielding decreased mixing and increased tortuosity (Toride et al., 2003; Torkzaban et al., 2006).

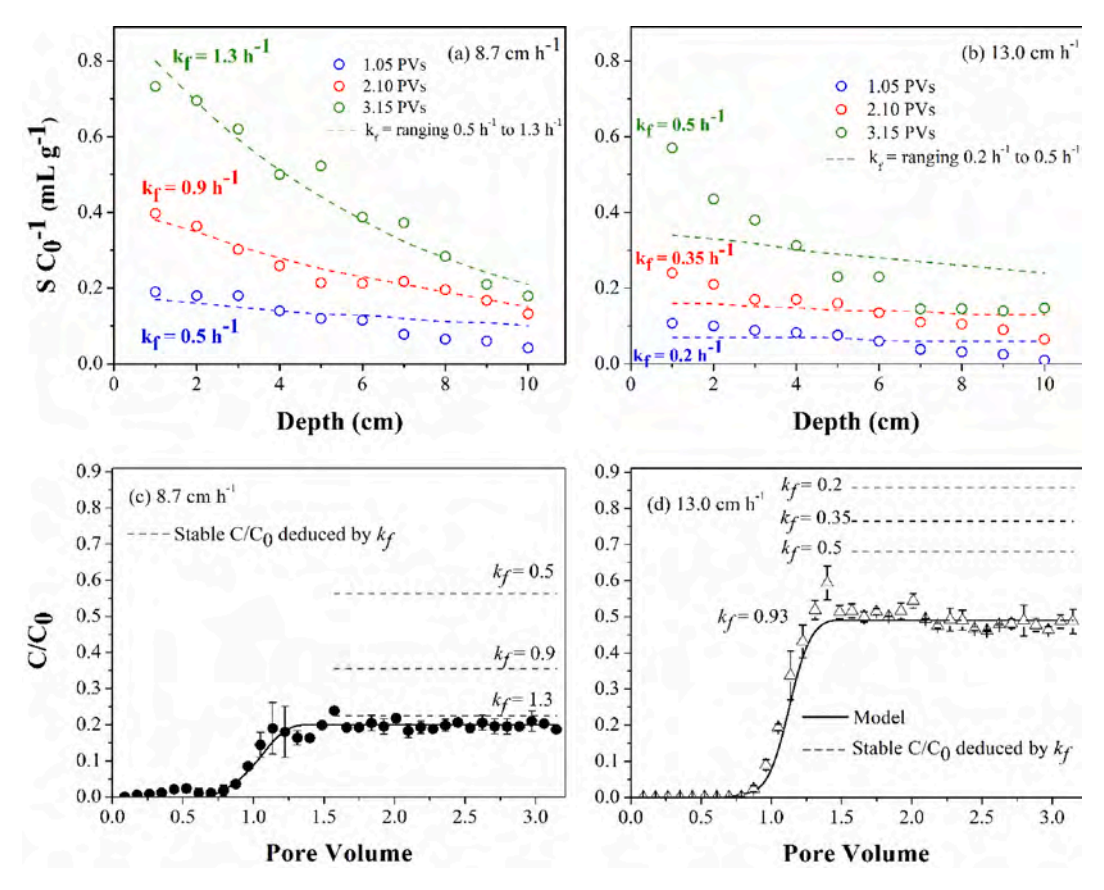


Fig. 5. (a) and (b) are simulations of bacterial distribution using multiple k_f (dotted colored lines) as a function of travel distance in quartz sand under saturated conditions. (c) and (d) are stable C/C_0 of breakthrough curves deduced by k_f under saturated conditions.

3.3. Bacterial transport under saturated and unsaturated flow conditions

Under saturated flow conditions, increasing pore water velocity from 8.7 cm h^{-1} to 13.0 cm h^{-1} reduced the percentage of retained bacteria (M_{ret}) from 77% to 58% (Table S1), increased the effluent bacteria recovered during breakthrough (M_{eff}), increased the relative concentration (C/C₀) during steady state breakthrough (Fig. 3), and decreased the average retained concentrations (Fig. 4).

The lower and slightly rising "steady-state" bacterial breakthrough C/C_0 under unsaturated relative to saturated flow conditions indicated greater retention of *E. coli* 652T7 when an AWI bounded a thinner water envelope surrounding grains in the porous media (Fig. 3). The recovery percentage of retained bacteria (M_{ret}) also increased under unsaturated relative to saturated conditions (from 77% to 84% at 8.7 cm h⁻¹ and 58% to 82% at 13.0 cm h⁻¹) (Table S1). In contrast to the saturated flow condition, there was negligible impact of pore water velocity on the values of steady state C/C_0 and M_{ret} (Fig. 3, Table S1), demonstrating that decreased pore water content decreased the influence of velocity on retention of *E. coli* 652T7.

3.4. Bacterial distribution under saturated and unsaturated flow conditions

Under saturated flow conditions, the concentrations of retained *E. coli* 652T7 decreased exponentially with migration distance from the entrance to the exit at the lower velocity (Fig. 4), as shown by quantification of k_f using Eqs. (2) and (3), respectively. The value of k_f increased slightly (but within typical factor of two-to-three experimental error) from $0.5 \, h^{-1}$ to $1.3 \, h^{-1}$ as the deposit was established from 1.05 to 3.15 pore volumes (Fig. 5) likely due to the presence of both mobile and retained bacteria (no elution). Equations (2) and (3) described well the

breakthrough and retained profiles under the lower velocity condition (8.7 cm h⁻¹) (Figs. 4 and 5), demonstrating that retention was described using a spatially-constant deposition rate, and that retention reflected compounded loss for each collector passed in the porous medium (Johnson, 2020). In contrast to the exponential retention profiles at lower pore water velocity, the profiles at higher pore water velocity were multi-exponential, as shown by the deviation of the data from the description provided by Eq. (3) (Fig. 5b). The term multi-exponential is used rather than hyper-exponential because it has been shown that the profiles can be described by superposed exponential distributions (e.g., Johnson et al., 2018). At the higher velocity, the values of k_f that described the retention profiles were a factor of two less than those that described the breakthrough curve (Fig. 5d), demonstrating a modest quantification discrepancy between direct observation of retention using the bioluminescence method and indirect detection from the effluent concentration. However, the method was sufficiently sensitive to describe the transition from exponential to multi-exponential profile with increased velocity.

Under unsaturated flow conditions, the distribution of *E. coli* 652T7 demonstrated a non-monotonic trend with migration distance (Fig. 6). The real-time images showed that the maximum concentration of retained bacteria shifted gradually towards the outlet as the bacteria were continuously injected. The distance of the maximum concentration of retained bacteria shifted down-gradient with increased PVs at both velocities. Such non-monotonic retention profiles contrasted with the exponential/multi-exponential profiles observed under saturated flow conditions, reflecting similar contrasts observed for bacteria as a function of ionic strength (Tong et al., 2005) and for carboxylate-modified polystyrene latex microspheres (CML) in glass beads versus quartz sand (Johnson et al., 2018), and for contrasting CML sizes in natural sand (Johnson, 2020).

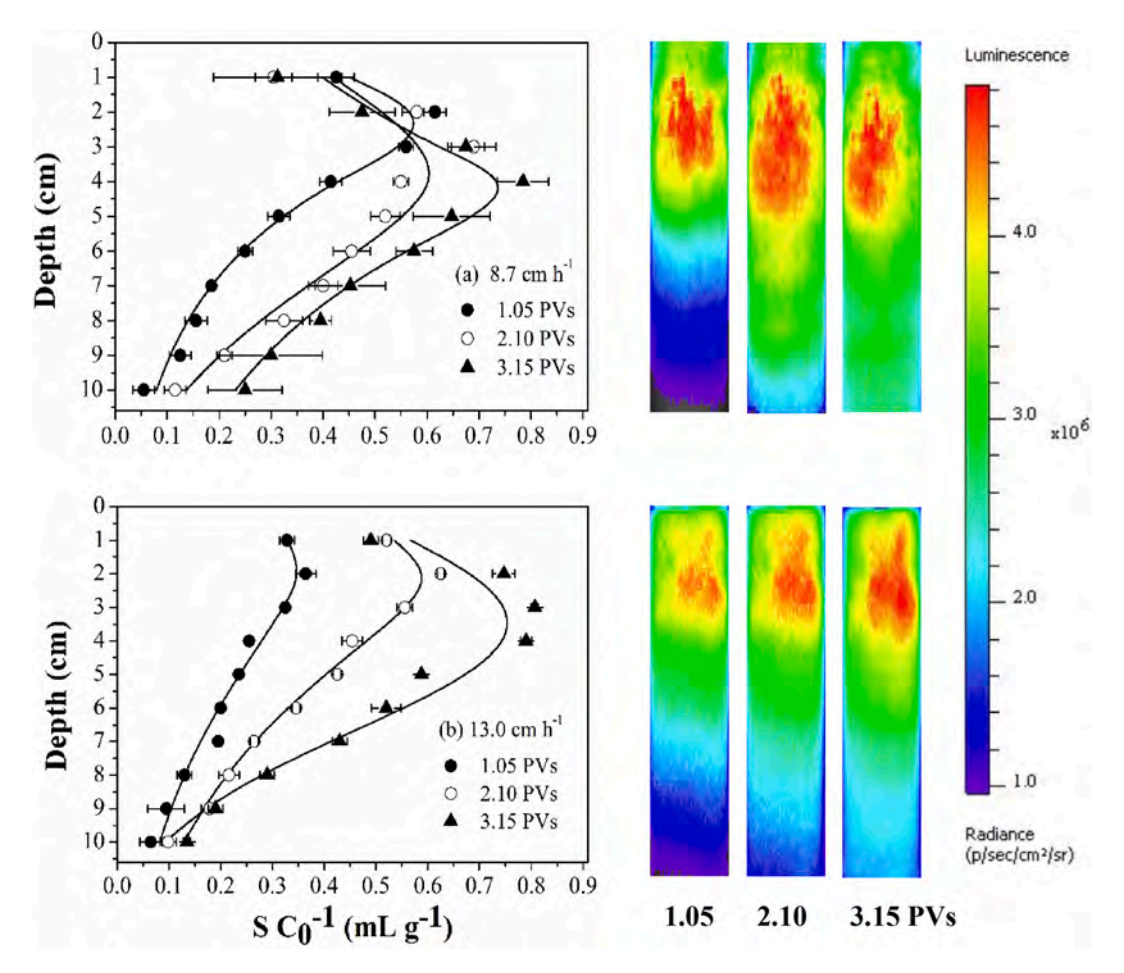


Fig. 6. The distribution of *E. coli* 652T7 with travel distance (i.e., depth) under unsaturated flow condition (85% saturation) at different pore water velocities (8.7 cm h^{-1} and 13.0 cm h^{-1}) in the porous media after 1.05, 2.10, and 3.15 pore volumes (PVs) of bacterial input. The fitted retention trend is shown by solid lines. The data (S C_0^{-1}) were acquired from the real-time images. The closer to the red part in the bioluminescent images, the higher the bacterial concentration was. Error bars represent the standard deviation of two replicates. (For interpretation of the references to colour in this figure legend, the reader is referred to the web version of this article.)

4. Discussion

4.1. Bacterial distribution under saturated flow conditions

The magnitudes of k_f under saturated flow conditions estimated using the Traj-Hap module in Parti-Suite (Table 1) were 4.5 h⁻¹ and 3.7 h⁻¹ for the 8.7 cm h⁻¹ and 13.0 cm h⁻¹ fluid velocities, respectively. These values were approximately a factor of four greater than those obtained from the experimentally-observed breakthrough (Fig. 5) using equation (2) (1.3 h⁻¹ for the 8.7 cm h⁻¹ velocity and 0.9 h⁻¹ for the 13.0 cm h⁻¹ velocity). This indicates that the bacterium-surface interactions at the SWI were somewhat unfavorable, agreeing with xDLVO calculations (Fig. S1, Table S2) which shows a significant (but not particularly large) barrier to attachment (260 kT) as well as a deep secondary minimum (–20 KT) where bacteria may associate with the surface without attachment.

The multi-exponential profile observed for the higher velocity under saturated flow conditions reflects an effective decrease in the deposition rate coefficient with distance of transport, which has been tentatively attributed to heterogeneity in surface properties among bacterial populations, yielding greater deposition of "stickier" bacteria upgradient of "less sticky" bacteria in the population (Albinger et al., 1994; Baygents et al., 1998; Simoni et al., 1998; Bolster et al., 2000; Redman et al., 2001; Tong and Johnson, 2007; Jouvet et al., 2018). Alternatively, bacterial retention in pore throats may reduce the effective pore throat size and increase subsequent filtration at the location (Shen et al., 2020),

although this temporal increase in retention should be reflected in decreased steady-state breakthrough (ripening) (Tong et al., 2008). That CML also display multi-exponential profiles drive the standing hypothesis that incomplete pore scale mixing produces fast- and slow-attaching subpopulations of otherwise identical individuals (Johnson et al., 2018; Johnson, 2020).

4.2. Bacterial distribution under unsaturated flow conditions

The increased M_{ret} under unsaturated conditions may reflect increased retention at either the AWI or at the SWI. Whereas previous studies indicate the AWI may attract cells, air being hydrophobic (Bradford and Torkzaban, 2008; Chen and Walker, 2012; Madumathi, et al., 2017), the Lifschitz-Van der Waals (combined Hamaker constant) and Lewis acid-base interactions were both repulsive for the AWI (Fig. S1).

The influence on η and k_f of decreased fluid shell thickness under unsaturated relative to saturated conditions was examined in the Traj-Hap module of Parti-Suite (Fig. S2), wherein the average thickness of the fluid envelope of the Happel collector was 56 μ m and 44 μ m under saturated and unsaturated conditions, respectively. In the trajectory simulations, the outer boundary of the fluid envelope was not treated as repulsive, such that the primary influence of unsaturated conditions was to increase the likelihood of intercepting the near surface fluid (secondary minimum) within which colloids may translate slowly downgradient without (or prior to) attachment (Johnson et al., 2018;

Table 1Parameters used in the pore-scale trajectories simulations.

| Parameters | meters 8.7 cm h^{-1} | | 13.0 cm h ⁻¹ | |
|---|--------------------------------|------------------------|----------------------------|-----------------------------|
| | Saturated | Unsaturated | Saturated | Unsaturated |
| Superficial velocity (m s ⁻¹) | 9.0×10^{-6} | 9.0×10^{-6} | 1.34×10^{-5} | 1.34×10^{-5} |
| Injection radius (m) | $1.2 	imes 10^{-4}$ | $8.0 	imes 10^{-5}$ | $1.2 	imes 10^{-4}$ | $8.0 	imes 10^{-5}$ |
| Happel porosity | 0.37 | 0.31 | 0.37 | 0.31 |
| Grain radius (m) | 3.38×10^{-4} | 3.38×10^{-4} | 3.38×10^{-4} | 3.38×10^{-4} |
| Colloid density (kg m^{-3}) | 1.05×10^3 | 1.05×10^3 | 1.05×10^3 | 1.05×10^3 |
| Fluid density (kg m^{-3}) | 9.98×10^2 | 9.98×10^2 | 9.98×10^{2} | 9.98×10^2 |
| Fluid viscosity (kg $m^{-1}s^{-1}$) | 9.98×10^4 | 9.98×10^4 | 9.98×10^4 | 9.98×10^4 |
| Hetmode | 1 | 1 | 1 | 1 |
| Large hetdomain radius | 0 | 0 | 0 | 0 |
| Ionic strength (mol m^{-3}) | 100 | 100 | 100 | 100 |
| Collector ζ potential (V) | -0.0244 | -0.0244 | -0.0244 | -0.0244 |
| Colloid ζ potential (V) | -0.0256 | -0.0256 | -0.0256 | -0.0256 |
| Combined Hamaker constant (J) | 6.5×10^{-21} | 6.5×10^{-21} | 6.5×10^{-21} | 6.5×10^{-21} |
| Van der Waals decay length (m) | 1.0×10^{-7} | 1.0×10^{-7} | 1.0×10^{-7} | 1.0×10^{-7} |
| Acid-base energy per area (J m ⁻²) | $^{-1.43}$ × $^{-5}$ | -1.43×10^{-5} | -1.43×10^{-5} | $^{-1.43}$ \times $^{-5}$ |
| Acid-base decay length (m) | 6×10^{-10} | 6×10^{-10} | 6×10^{-10} | 6×10^{-10} |
| Steric energy per area (J m ⁻²) | 1.7×10^{-12} | 1.7×10^{-12} | 1.7×10^{-12} | 1.7×10^{-12} |
| Steric decay length (m) | 4.1 × 10 ⁻¹⁰ | 4.1×10^{-10} | 4.1 × 10 ⁻¹⁰ | 4.1×10^{-10} |
| Multiplier of diffusion force (-) | 1.35 | 1.35 | 1.35 | 1.35 |
| Multiplier of gravity force | 1.00 | 1.00 | 1.00 | 1.00 |

Johnson, 2020). The simulated values of k_f were approximately 15% to 20% larger under unsaturated relative to saturated conditions, increasing from $4.5 \, h^{-1}$ to $5.2 \, h^{-1}$ at the lower velocity ($8.7 \, \text{cm h}^{-1}$) and from $3.7 \, h^{-1}$ to $4.4 \, h^{-1}$ at the higher velocity ($13.0 \, \text{cm h}^{-1}$). This modest increase in simulated k_f from saturated to unsaturated conditions is consistent with the observed decrease in breakthrough (Fig. 3) and increase in retained mass (Table S1) under unsaturated relative to saturated conditions.

In contrast, the trajectory simulations predict slightly decreased k_f with increased velocity under unsaturated conditions (from 5.2 h⁻¹ to 4.4 h⁻¹); however, no obvious increase in retention with increased velocity was observed in the breakthrough concentrations under unsaturated conditions (Fig. 3). This discrepancy suggests that increased retention under unsaturated conditions may not have been primarily driven by bacterial accumulation in secondary minima, but may instead have involved retention by capillary forces at the AWI, which can also produce slow down-gradient translation of bacteria (Bradford et al., 2006, 2007; Tong et al., 2008; Torkzaban et al., 2008; Sen, 2011), as driven by capillary fringe fluctuations (Noordmans et al., 1997; Gómez-Suárez et al., 1999, 2000; Sharma et al., 2008; Aramrak et al., 2011, 2014; Lazouskaya et al., 2011; Aramrak et al., 2011, 2014). Whereas the average fluid shell thickness (44 μm) greatly exceeds bacterial size, this average does not account for the large fluid shell thickness at grain contacts (pendant water) and lesser fluid shell thickness away from grain contacts, where there may be decreased dependence on fluid drag, sedimentation, and diffusion to bring bacteria into proximity with either interface.

The real-time observation of bacterial distribution from source provided by the bioluminescence method showed that the shapes of the

profiles (exponential, multi-exponential, non-monotonic) remained temporally consistent and did not evolve from one form into another as deposition continued. This novel observation indicates that the predominance of particular mechanisms of retention remained consistent as deposition proceeded, whereas this predominance shifted with modest change in velocity and saturation.

5. Conclusion

Bioluminescent imaging as performed here *via* the IVIS Spectrum was demonstrated as an effective method for real-time observation of bacterial distribution and evolution of these profiles during transport through porous media under different flow conditions. The range of outcomes from exponential to multi-exponential to non-monotonic distributions was observed with changes in flow velocity and pore water saturation. Non-monotonic distribution reflected bacterial accumulation without arrest in either the secondary minimum at the SWI and/or capillary interaction at the AWI. This novel real-time observation method showed that the forms of the distributions remained consistent as deposition continued. These results provide critical information for understanding and predicting the spatiotemporal heterogeneity of bacterial transport behaviors through porous media including deep-bed filters and aquifer sediments.

Author contributions

LY analyzed the data and wrote the manuscript. JK performed the experiments. JZ designed the experiments and revised the manuscript. XC provided financial support and experimental facilities for the research, SAR provided bioluminescent bacteria and edited the manuscript. WPJ guided in the data modeling, edited the manuscript, and assisted in result interpretation.

Declaration of Competing Interest

The authors declare that they have no known competing financial interests or personal relationships that could have appeared to influence the work reported in this paper.

Acknowledgments

This work was financially supported by the National Natural Science Foundation of China (Grant No. 41730858).

Appendix A. Supplementary data

Supplementary data to this article can be found online at https://doi.org/10.1016/j.jhydrol.2021.126603.

References

Adadevoh, J.S.T., Ramsburg, C.A., Ford, R.M., 2018. Chemotaxis increases the retention of bacteria in porous media with residual NAPL entrapment. Environ. Sci. Technol. 52 (13), 7289–7295.

Albinger, O., Biesemeyer, B.K., Arnold, R.G., Logan, B.E., 1994. Effect of bacterial heterogeneity on adhesion to uniform collectors by monoclonal populations. FEMS Microbiol. Lett. 124 (3), 321–326.

Aramrak, S., Flury, M., Harsh, J.B., 2011. Detachment of deposited colloids by advancing and receding air-water interfaces. Langmuir. 27 (16), 9985–9993.

Aramrak, S., Flury, M., Harsh, J.B., Zollars, R.L., 2014. Colloid mobilization and transport during capillary fringe fluctuations. Environ. Sci. Technol. 48 (13), 7272–7279.

Bai, H., Cochet, N., Pauss, A., Lamy, E., 2016. Bacteria cell properties and grain size impact on bacteria transport and deposition in porous media. Colloids Surf. B: Biointerfaces. 139 (1), 148–155.

Balkhair, K.S., 2017. Modeling fecal bacteria transport and retention in agricultural and urban soils under saturated and unsaturated flow conditions. Water Res. 110 (1), 313–320

Baygents, J.C., Glynn Jr, J.R., Albinger, O., Biesemeyer, B.K., Ogden, K.L., Arnold, R.G., 1998. Variation of surface charge density in monoclonal bacterial populations: implications for transport through porous media. Environ. Sci. Technol. 32 (11), 1596–1603.

- Bolster, C.H., Mills, A.L., Hornberger, G., Herman, J., 2000. Effect of intra-population variability on the long-distance transport of bacteria. Ground Water. 38 (3), 370–375
- Bradford, S.A., Simunek, J., Walker, S.L., 2006. Transport and straining of *E. coli* O157: H7 in saturated porous media. Water Resour. Res. 42 (12), W12S12.
- Bradford, S.A., Torkzaban, S., 2008. Colloid transport and retention in unsaturated porous media: A review of interface-, collector-, and pore-scale processes and models. Vadose Zone J. 7 (2), 667–681.
- Bradford, S.A., Torkzaban, S., Walker, S.L., 2007. Coupling of physical and chemical mechanisms of colloid straining in saturated porous media. Water Res. 41 (13), 3012–3024.
- Chen, G., Walker, S.L., 2012. Fecal indicator bacteria transport and deposition in saturated and unsaturated porous media. Environ. Sci. Technol. 46 (16), 8782–8790.
- Engström, E., Thunvik, R., Kulabako, R., Balfors, B., 2015. Water transport, retention, and survival of *Escherichia coli* in unsaturated porous media: A comprehensive review of processes, models, and factors. Crit. Rev. Env. Sci. Tec. 45 (1), 1–100.
- Firouzi, A.F., Homaee, M., Klumpp, E., Kasteel, R., Tappe, W., 2015. Bacteria transport and retention in intact calcareous soil columns under saturated flow conditions. J. Hydrol. Hydromech. 63 (2), 102–109.
- Gómez-Suárez, C., Noordmans, J., van der Mei, H.C., Busscher, H.J., 1999. Removal of colloidal particles from quartz collector surfaces as simulated by the passage of liquid-air interfaces. Langmuir. 15 (15), 5123–5127.
- Gómez-Suárez, C., Van Der Mei, H.C., Busscher, H.J., 2000. Air bubble-induced detachment of positively and negatively charged polystyrene particles from collector surfaces in a parallel-plate flow chamber. J. Adhes. Sci. Technol. 14 (12), 1527-1537
- Johnson, W. P., 2020. Quantitative linking of nanoscale interactions to continuum-scale nanoparticle and microplastic transport in environmental granular media. Environ. Sci. Technol. 10.1021/acs.est.0c01172.
- Johnson, W.P., Rasmuson, A., Pazmiño, E., Hilpert, M., 2018. Why variant colloid transport behaviors emerge among identical individuals in porous media when colloid-surface repulsion exists. Environ. Sci. Technol. 52 (13), 7230–7239.
- Jouvet, L., Rodríguez-Rojas, A., Steiner, U.K., 2018. Demographic variability and heterogeneity among individuals within and among clonal bacteria strains. Oikos. 127 (5), 728–737.
- Keller, A.A., Auset, M., 2007. A review of visualization techniques of biocolloid transport processes at the pore scale under saturated and unsaturated conditions. Adv. Water Resour. 30 (6-7), 1392–1407.
- Lazouskaya, V., Wang, L.-P., Gao, H., Shi, X., Czymmek, K., Jin, Y., 2011. Pore-scale investigation of colloid retention and mobilization in the presence of a moving airwater interface. Vadose Zone J. 10 (4), 1250–1260.
- Li, X., Lin, C.-L., Miller, J.D., Johnson, W.P., 2006. Pore-scale observation of microsphere deposition at grain-to-grain contacts over assemblage-scale porous media domains using x-ray microtomography. Environ. Sci. Technol. 40 (12), 3762–3768.
- Liu, Y., Yang, C.-H., Li, J., 2007. Influence of extracellular polymeric substances on Pseudomonas aeruginosa transport and deposition profiles in porous media. Environ. Sci. Technol. 41 (1), 198–205.
- Logan, B.E., Jewett, D.G., Arnold, R.G., Bouwer, E.J., O'Melia, C.R., 1995. Clarification of clean-bed filtration models. J. Environ. Eng. 121 (12), 869–873.
- Long, W., Hilpert, M., 2009. A correlation for the collector efficiency of Brownian particles in clean-bed filtration in sphere packings by a Lattice-Boltzmann method. Environ. Sci. Technol. 43 (12), 4419–4424.
- Ma, E., Ouahbi, T., Wang, H., Ahfir, N.-D., Alem, A., Hammadi, A., 2018. Modeling of the transport and deposition of polydispersed particles: effects of hydrodynamics and spatiotemporal evolution of the deposition rate. Environ. Pollut. 237, 1011–1022.
- Ma, H., Pedel, J., Fife, P., Johnson, W.P., 2009. Hemispheres-in-cell geometry to predict colloid deposition in porous media. Environ. Sci. Technol. 43 (22), 8573–8579.
- Madumathi, G., Philip, L., Bhallamudi, S. M., 2017. Transport of E.coli in saturated and unsaturated porous media: effect of physiological state and substrate availability. Sadhana-acad. P. Eng. S. 42 (6), 1007-1024.
- Molnar, I.L., Johnson, W.P., Gerhard, J.I., Willson, C.S., O'Carroll, D.M., 2015. Predicting colloid transport through saturated porous media: A critical review. Water Resour. Res. 51 (9), 6804–6845. https://doi.org/10.1002/2015WR017318.
- Nelson, K.E., Ginn, T.R., 2011. New collector efficiency equation for colloid filtration in both natural and engineered flow conditions. Water Resour. Res. 47, W05543.

- Noordmans, J., Wit, P.J., Van Der Mei, H.C., Busscher, H.J., 1997. Detachment of polystyrene particles from collector surfaces by surface tension forces induced by airbubble passage through a parallel plate flow chamber. J. Adhes. Sci. Technol. 11 (7), 957–969.
- Rajagopalan, R., Tien, C., 1976. Trajectory analysis of deep-bed filtration with the sphere-in-cell porous media mode. AIChE J. 22 (3), 523–533.
- Redman, J.A., Grant, S.B., Olson, T.M., Estes, M.K., 2001. Pathogen filtration, heterogeneity, and the potable reuse of wastewater. Environ. Sci. Technol. 35 (9), 1798–1805.
- Redman, J.A., Walker, S.L., Elimelech, M., 2004. Bacterial adhesion and transport in porous media: role of the secondary energy minimum. Environ. Sci. Technol. 38 (6), 1777–1785
- Rockhold, M.L., Yarwood, R.R., Niemet, M.R., Bottomley, P.J., Brockman, F.J., Selker, J. S., 2007. Visualization and modeling of the colonization dynamics of a bioluminescent bacterium in variably saturated, translucent quartz sand. Adv. Water Resour. 30 (6-7), 1593–1607.
- Sasidharan, S., Bradford, S.A., Torkzaban, S., Ye, X., Vanderzalm, J., Du, X., Page, D., 2017. Unraveling the complexities of the velocity dependency of *E. coli* retention and release parameters in saturated porous media. Sci. Total Environ. 603-604, 406–415.
- Sen, T.K., 2011. Processes in pathogenic biocolloidal contaminants transport in saturated and unsaturated porous media: A review. Water Air Soil Poll. 216 (1-4), 239–256.
- Sharma, P., Flury, M., Zhou, J., 2008. Detachment of colloids from a solid surface by a moving air-water interface. J. Colloid Interface Sci. 326 (1), 143–150.
- Shen, C., Jin, Y., Zhuang, J., Li, T., Xing, B., 2020. Role and importance of surface heterogeneities in transport of particles in saturated porous media. Crit. Rev. Env. Sci. Tec. 50 (3), 244–329.
- Shi, W.-J., Menn, F.-M., Xu, T., Zhuang, Z.T., Beasley, C., Ripp, S., Zhuang, J., Layton, A. C., Sayler, G.S., 2014. C60 reduces the bioavailability of mercury in aqueous solutions. Chemosphere. 95, 324–328.
- Simoni, S.F., Harms, H., Bosma, T.N.P., Zehnder, A.J.B., 1998. Population heterogeneity affects transport of bacteria through sand columns at low flow rates. Environ. Sci. Technol. 32 (14), 2100–2105.
- Tong, M., Camesano, T.A., Johnson, W.P., 2005. Spatial variation in deposition rate coefficients of an adhesion-deficient bacterial strain in quartz sand. Environ. Sci. Technol. 39 (10), 3679–3687.
- Tong, M., Johnson, W.P., 2006. Excess colloid retention in porous media as a function of colloid size, fluid velocity, and grain angularity. Environ. Sci. Technol. 40 (24), 7725–7731.
- Tong, M., Johnson, W.P., 2007. Colloid population heterogeneity drives hyperexponential deviation from classic filtration theory. Environ. Sci. Technol. 41 (2), 493–499.
- Tong, M., Ma, H., Johnson, W.P., 2008. Funneling of flow into grain-to-grain contacts drives colloid-colloid aggregation in the presence of an energy barrier. Environ. Sci. Technol. 42 (8), 2826–2832.
- Torkzaban, S., Hassanizadeh, S.M., Schijven, J.F., de Bruin, H.A.M., de Roda Husman, A. M., 2006. Virus transport in saturated and unsaturated sand columns. Vadose Zone J. 5 (3), 877–885.
- Torkzaban, S., Tazehkand, S.S., Walker, S.L., Bradford, S.A., 2008. Transport and fate of bacteria in porous media: coupled effects of chemical conditions and pore space geometry. Water Resour. Res. 44 (4), W04404.
- Toride, N., Inoue, M., Leij, F.J., 2003. Hydrodynamic dispersion in an unsaturated dune sand. Soil Sci Soc Am. 67, 703–712.
- Tufenkji, N., Elimelech, M., 2004. Correlation equation for predicting single-collector efficiency in physicochemical filtration in saturated porous media. Environ. Sci. Technol. 38 (2), 529–536.
- Yao, K.-M., Habibian, M.T., O'Melia, C.R., 1971. Water and waste water filtration. Concepts and applications. Environ. Sci. Technol. 5 (11), 1105–1112.
- Zhang, H., Zeng, H., Ulrich, A.C., Liu, Y., 2016. Comparison of the transport and deposition of *Pseudomonas aeruginosa* under aerobic and anaerobic conditions. Water Resour. Res. 52 (2), 1127–1139.
- Zhuang, J., Liu, W., Yang, L., Kang, J., Zhang, X., 2020. Bioluminescent imaging and tracking of bacterial transport in soils. Bioluminescent Imaging and Tracking of Bacterial Transport in Soils. Methods in Molecular Biology - Bioluminescent Imaging 2081, 53–65. https://doi.org/10.1007/978-1-4939-9940-8_5.